Vienna Mapping Functions

J. Boehm and H. Schuh

Institute of Geodesy and Geophysics (IGG), TU Vienna, Austria

Summary: Recently, numerical weather models NWMs have been investigated to improve mapping functions which are used for tropospheric modelling in VLBI and GPS data analyses. E.g., the Vienna mapping functions VMF are based on direct raytracing through NWMs without taking any intermediate parameters. In this study, pressure level data from ECMWF (European Centre for Medium-Range Weather Forecasts) are used. Two approaches are introduced to derive the coefficients for the continued fraction forms of the mapping functions: Whereas the 'rigorous approach' is rather time consuming, the 'fast approach' needs only one raytrace per epoch and site. Used for VLBI analyses, the VMFs improve the repeatability of baseline lengths by up to 10% compared to mapping functions without input from NWMs. Elevation angle cutoff tests with the VMFs reveal that there might be systematic effects that have not been visible with prior mapping functions.

1 Introduction

Raytracing through radiosonde data has often been used to develop and validate mapping functions which are used for tropospheric modelling in VLBI and GPS data analyses. E.g., the New Mapping Functions NMF (Niell, 1996), which need the station height, the station latitude and the day of the year as input parameters, were developed using radiosonde data over a wide range of latitudes.

In the past years, a lot of effort has been put into the development of mapping functions which are based on data from numerical weather models (NWMs). Niell (2001b) set up the 'isobaric' mapping functions IMF which apply as input parameters the height of the 200 mbar pressure level ('z200') and the ratio of the wet path delay along a straight line at 3.3° elevation and its zenith delay ('smfw3'). But still, the equations for the coefficients of the continued fraction form (see Eq. 1) are based on raytracing through radiosonde data.

When working on the implementation of these mapping functions with pressure level data from the ECMWF (European Centre for Medium-Range Weather Forecasts) it became evident that the NWMs could be exploited more rigorously by discarding intermediate parameters like z200 and smfw3. The main idea for the Vienna Mapping Functions VMF is to simply use the raytracing through the NWM directly instead of taking intermediate steps.

To illustrate the accuracy of NWMs and the raytracing program (see Appendix A), Figures 1a and 1b show the hydrostatic and wet mapping functions at 5° elevation derived from radiosonde data and ECMWF pressure level data at a site in Vienna ('Hohe Warte') in the year 2002. The pressure level data consist of 15 levels whereas the radiosonde data used here comprises at least 50 levels. There is a very good agreement between the time series. If multiplied by 2300 mm, the difference in the hydrostatic mapping function is 4.1 ± 6.5 mm. The wet mapping functions (multiplied by 200 mm) differs by -0.3 mm $\pm$ 4.1 mm. It has to be mentioned that the same radiosonde data have been used to determine the ECMWF pressure levels.

Thus, the total agreement is still at the 1 cm level at 5° elevation what implies that the mapping functions can be calculated directly from raytracing through ECMWF pressure level data, at least if the pressure level data include meteorological information of sufficient accuracy at the site (e.g. from nearby radiosonde launches). This presumption is the basis for the concept of the Vienna mapping functions VMF. Tests with independent radiosonde data, i.e., that were not used for the determination of the ECMWF pressure level data would be desirable and remain to be done.

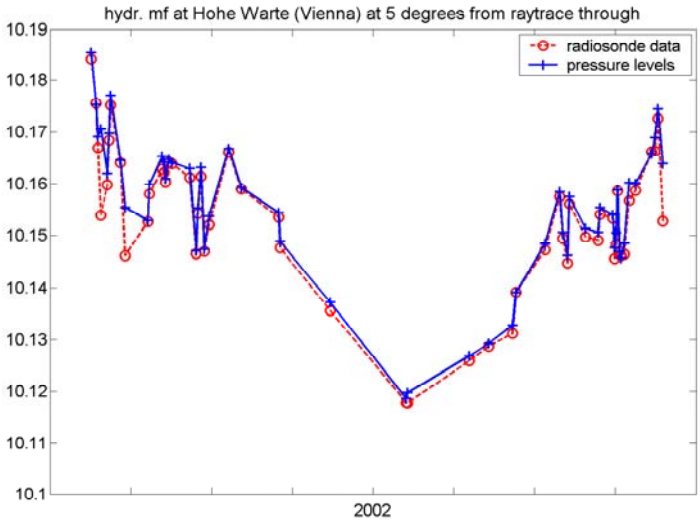

Figure 1a: Hydrostatic mapping functions at 5° elevation calculated from raytracing through radiosonde data and ECMWF pressure level data for identical epochs in 2002 for a site in Vienna ('Hohe Warte'). The seasonal variation can be clearly seen.

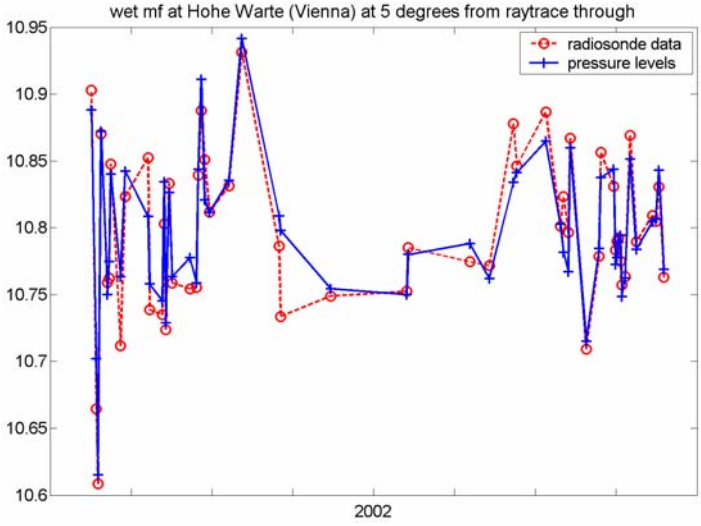

Figure 1b: Wet mapping functions at 5° elevation calculated from raytracing through radiosonde data and ECMWF pressure level data for identical epochs in 2002 for a site in Vienna ('Hohe Warte').

2 Determination of the Vienna Mapping Functions (VMF)

The continued fraction form which is used for the hydrostatic and wet mapping function is shown in Eq. (1). This form is also used in the NMF (Niell, 1996) and in the IMF (Niell, 2001b).

$$\mathrm{mf}(e) = \frac{1+\dfrac{a}{1+\dfrac{b}{1+c}}}{\sin e+\dfrac{a}{\sin e+\dfrac{b}{\sin e+c}}} \qquad (1)$$

Table 1: Input parameters for hydrostatic and wet mapping functions. φ is the station latitude, h is the station height and doy is the day of the year.

	NMF	IMF	VMF
hyd.	doy, h, φ	z200, φ, h	h, a (,b, c)
wet	φ	smfw3, h	a (,b, c)

Three coefficients a, b and c are sufficient to map zenith delays down to elevations of 3°. In the case of VMF, these coefficients have to be determined from raytracing through NWMs. The raytracing is described in Appendix A. Input parameters for the raytracing program are an initial elevation angle e_0, and values for height, temperature and water vapour pressure at 15 distinct pressure levels. The raytracing then yields the outgoing (= vacuum) elevation angle e, and the values for the hydrostatic and the wet mapping function. The hydrostatic mapping function includes the geometric bending effect.

Two ways of determining the coefficients from raytracing through ECMWF pressure levels will be presented here. The first one is the rigorous and very accurate way, whereas the second one is faster and still sufficiently accurate.

2.1 Rigorous determination of the coefficients

For each site (e.g. VLBI station) and each epoch when ECMWF pressure level data are available , i.e. every six hours, the hydrostatic and wet mapping functions as well as the outgoing (= vacuum) elevation angles are determined by raytracing through the pressure levels at ten different initial elevation angles (90°, 70°, 50°, 30°, 20°, 15°, 10°, 7°, 5°, 3.3°). Then, the coefficients a, b and c for the continued fraction forms (Eq. 1) for the hydrostatic and wet mapping functions are estimated in a least-squares procedure. The adjustment shows that three coefficients are enough to map down the zenith delays to 3° elevation. So, at each site a time series of six parameters (a_h, b_h, c_h, a_w, b_w, c_w) exists with a resolution of six hours. The rigorous approach is not well-suited to be used on a global grid because raytracing still takes a lot of computing time. Furthermore, it remains to be tested whether information gets lost by the spatial interpolation of the parameters a, b and c.

2.2 Fast determination of the coefficient a

Although computers are very fast today, raytracing is still time consuming, especially if it has to be performed on a global grid, four times per day and ten times per grid point. For this reason, a fast version of the rigorous way has been developed that yields similar values for the mapping functions. Instead of determining the raytracing at ten different elevation angles, the raytracing is only calculated for one initial elevation angle of 3.3°. This yields one value for the hydrostatic, one for the wet mapping function and the vacuum elevation angle (~3°). Then, predefined formulas are used for the b and c coefficients, and the coefficients a can be determined by simply inverting the continued fraction form (Eq. 1). For the hydrostatic mapping function the coefficients b_h and c_h are taken from the hydrostatic part of the isobaric mapping function IMF. If φ is the geodetic latitude, the coefficients are determined by:

$$b_h = 0.002905 \tag{2}$$

$$c_h = 0.0634 + 0.0014 \cdot \cos(2\varphi) \tag{3}$$

For the wet part the coefficients b_h and c_w are taken from NMF (valid for φ = 45°):

$$b_w = 0.00146 \tag{4}$$

$$c_w = 0.04391 \tag{5}$$

Contrarily to the rigorous approach, a height correction is applied for the hydrostatic part according to Niell (1996), in order to refer the hydrostatic coefficients a_h to zero height. The advantage is that the spatial interpolation yields better results when all grid points are referred to zero height. On the other hand, this height correction has to be re-applied when using the hydrostatic mapping function.

3 Validation of the VMF

3.1 Comparison of mapping function values for CONT02

The Continuous VLBI 2002 program of the IVS (CONT02) consists of 15 consecutive 24 h VLBI experiments with the same 8 stations throughout: Algonquin, Gilmore Creek, HartRAO, Kokee Park, Ny Alesund, Wettzell, Westford, and Onsala. The sessions last from October 16 to October 30, 2002.

For this time span, the mapping function values from NMF, IMF and VMF (fast approach) are compared to those from VMF (rigorous approach). If the unit of the mapping functions is length, they refer to 2300 mm hydrostatic and 200 mm wet zenith delay. Table 2 summarizes the rms-differences for an elevation angle of 5°. If the rigorous approach was correct i.e., if the NWM was perfect, the rms-differences at 5° elevation are 1 cm, 3 cm and 5 cm for VMF (fast), IMF and NMF, respectively. Following a rule of thumb (Niell et al., 2001a), one-third of the mapping function error at the lowest elevation angle included in the analysis can be seen as station height error. So, these rms-differences would correspond to 3 mm, 1 cm and 1.7 cm station height error if the NWM was error-free.

Table 2: Rms-differences in mm of VMF (fast), IMF and NMF compared to the rigorous approach of VMF for the duration of CONT02. The total (hydrostatic plus wet) rms-differences are at about 1 cm, 3 cm and 5 cm, respectively.

Site	hydrostatic at 5° in [mm]			wet at 5° in [mm]		
	VMF (fast)	IMF	NMF	VMF (fast)	IMF	NMF
Algopark	7	18	67	1	7	14
Gilcreek	12	18	20	1	8	15
HartRAO	4	25	19	1	7	17
Kokee	2	29	23	1	5	21
Nyales20	19	34	52	0	8	12
Wettzell	8	16	34	1	7	18
Westford	4	18	48	1	8	15
Onsala60	11	12	39	1	8	19

3.2 Baseline length repeatabilities

Improved mapping functions are expected to yield improved geodetic accuracies. A good measure for the quality of geodetic results is the baseline length repeatability.

For the VLBI analysis, the classical least-squares method (Gauss-Markov model) of the OCCAM 5.1 VLBI software package (Titov et al., 2001) is used. Free network solutions are calculated for the 24 h sessions with five Earth orientation parameters being estimated (nutation, dUT1 and pole coordinates). Atmospheric loading parameters are taken from Petrov and Boy (2003), and total gradient offsets are estimated every 6 hours using the model by MacMillan (1995).

Baseline length repeatabilities are determined for CONT02, and for all IVS-R1 and IVS-R4 sessions until March, 2003. For the following investigations no baselines are used which include the station Tigo Concepcion (Chile) and the station at Gilmore Creek after the Earthquake on November 3, 2002. Figure 2 shows the baseline length repeatabilities for the IVS-R1 sessions with a cutoff angle of 5° elevation. A significant improvement of nearly 10% can be seen for the VMF (fast) as well as for the IMF when compared to NMF.

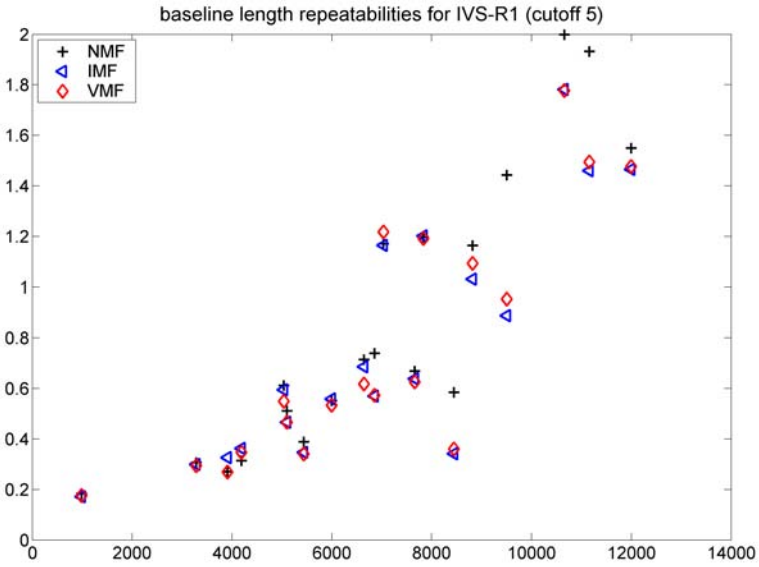

Figure 2: Baseline length repeatabilities in cm for the IVS-R1 sessions until March, 2003. A significant improvement can be seen for the VMF (fast) and the IMF i.e., the mapping functions that are based on data from NWMs when compared to the NMF.

Tables 3a and 3b provide information about the improvement of the baseline length repeatabilities of the CONT02, IVS-R1 and IVS-R4 sessions with VMF (fast) and IMF compared to NMF. Table 3a gives the percentage of improved baselines, and Table 3b provides the mean value of the relative improvement over all baselines. The cutoff elevation angle was set to 5°.

Table 3a: Baselines with better repeatabilities in %. A clear majority of the baselines is improved with the mapping functions based on NWMs.

	CONT02	IVS-R1	IVS-R4
IMF	54 %	79 %	62 %
VMF (fast)	70 %	89 %	62 %

Table 3b: Mean values of the relative improvements in %. The repeatabilities with VMF (fast) are slightly better than the repeatabilities with IMF. The improvement is largest for the IVS-R1 sessions (almost 10 %).

	CONT02	IVS-R1	IVS-R4
IMF	1.9 %	8.3 %	3.0 %
VMF (fast)	5.2 %	9.7 %	3.5 %

Figure 3 shows the station height repeatabilities for CONT02. Six out of eight (75%) of the station height repeatabilities are improved for IMF and VMF (fast) compared to NMF. The mean relative improvement is 7.2% for IMF and 10.7% for VMF (fast). For this investigation the horizontal station components were fixed to ITRF2000 and the station heights were estimated. It has to be clearly stated that the station height repeatability at one station is also effected by changes in the mapping functions at the other stations. Nevertheless, the main part of the changed repeatability is due to the mapping function used at the station itself. Figure 3 shows that only at HartRAO (South Africa) the repeatability gets slightly worse when using IMF or VMF (fast). This is likely due to the fact that the ECMWF pressure level data is lacking good input information in this area. Detailed investigations reveal that the improvement of repeatabilities for baselines lengths including HartRAO is not as big as for the other baselines.

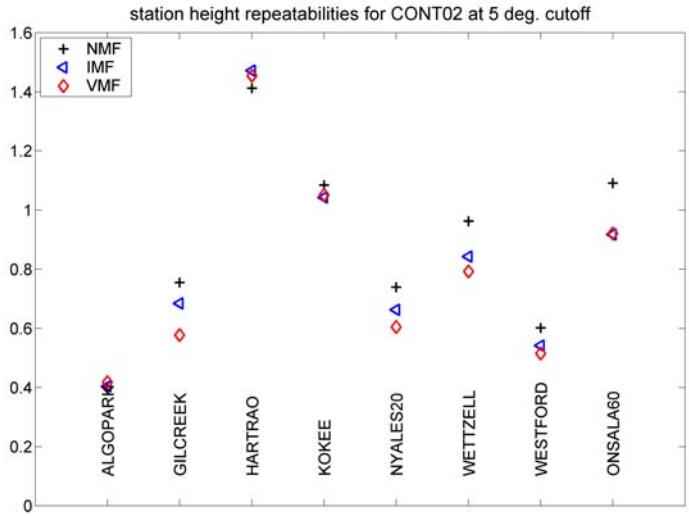

Figure 3: Station height repeatabilities in cm for CONT02. 75% of the station height repeatabilities are improved for IMF and VMF (fast) compared to NMF. The relative improvement (mean for all stations) is 7.2% for IMF and 10.7% for VMF (fast).

3.3 Elevation angle cutoff tests

Another measure for the quality of mapping functions can be obtained by elevation angle cutoff tests. These tests show how baseline lengths change when the cutoff elevation angle is varied. In Figures 4a, 4b and 4c the changes of the baseline lengths are plotted for the cutoff elevation angle 5° compared to 7° and 10° for CONT02. The plots are for NMF, IMF and VMF (fast), respectively and the changes themselves are well below the repeatabilities. The triangle in the upper right of all three plots 4a, 4b and 4c corresponds to 10° elevation cutoff (compared to 5°) on the baseline HartRAO to Kokee Park. Due to its length of almost one Earth diameter obviously too many observables get 'lost' when increasing the cutoff elevation angle from 5° to 10°.

In general, for the NMF (Fig. 4a) the variation of the baseline lengths is rather large for the 10° cutoff (between -0.6 mm and +0.2 mm). For the IMF (Fig. 4b) when increasing the cutoff elevation angle the scatter of the baseline lengths is getting smaller than for NMF, but a systematic effect becomes visible: The longer the baselines are, the shorter the baselines get with higher cutoff elevation angles. With VMF (fast) (Fig. 4c), this systematic effect becomes even more evident for the 10° cutoff solutions. For illustration a quadratic regression polynomial was fitted to the differences.

.

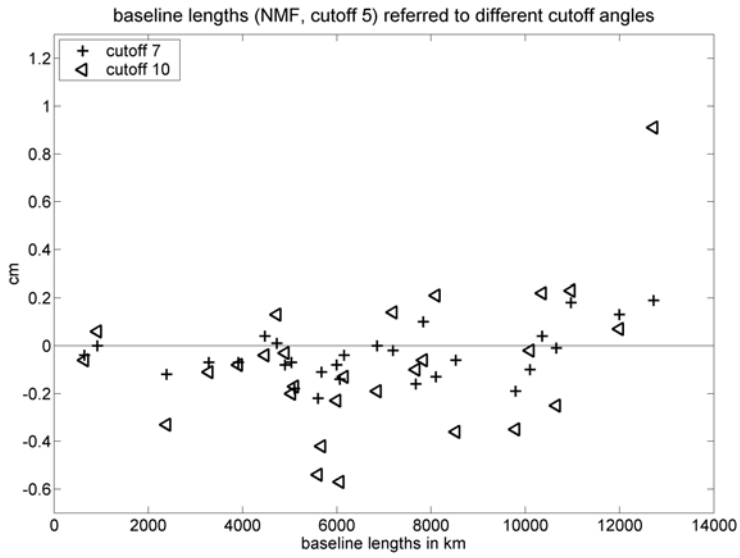

Figure 4a: Elevation angle cutoff test for CONT02 and NMF. Baseline lengths with a 5° cutoff elevation angle are compared to baseline lengths with a 7° and 10° cutoff elevation angle.

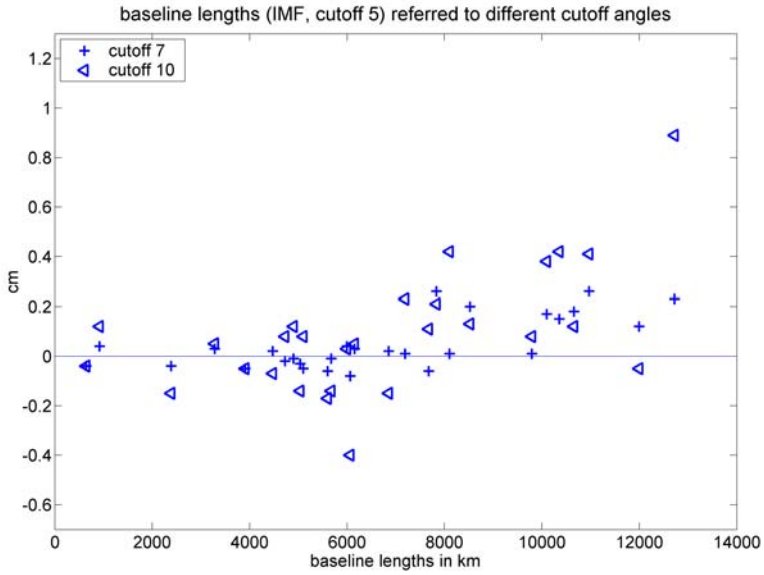

Figure 4b: Elevation angle cutoff test for CONT02 and IMF. Baseline lengths with a 5° cutoff elevation angle are compared to baseline lengths with a 7° and 10° cutoff elevation angle. A systematic effect might be seen for longer baselines.

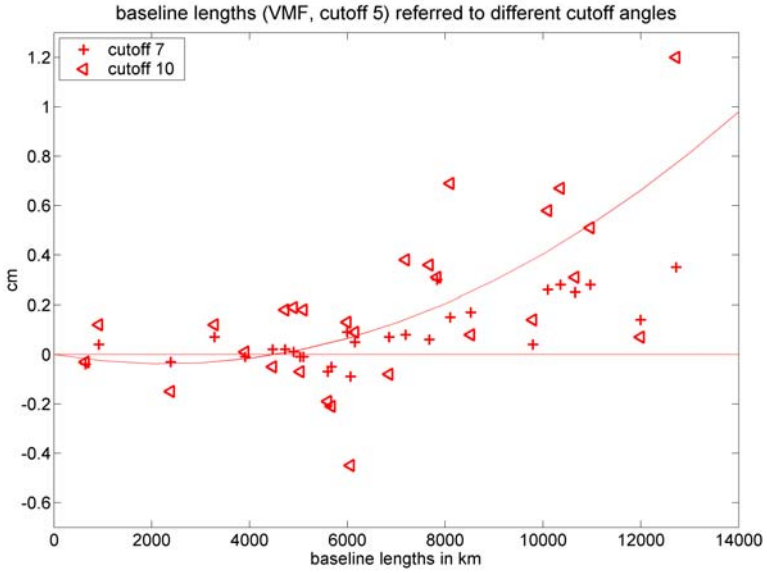

Figure 4c: Elevation angle cutoff test for CONT02 and VMF (fast). Baseline lengths with a 5° cutoff elevation angle are compared to baseline lengths with a 7° and 10° cutoff elevation angle. For illustration of the systematic effect a quadratic polynomial is fitted to the differences.

In spite of the reduced scatter, systematic effects could indicate problems with the mapping function. In the case of VMF (fast), a possible error source might be errors in the raytracing program. There could be other reasons as well, e.g. deficiencies in the gradient model for observations at low elevations.

Figures 5a and 5b show the cutoff elevation angle tests for IVS-R1 and IVS-R4 in the sense cutoff 5° minus cutoff 10°. Whereas IVS-R4 clearly confirms the assumption of systematic effects, it is not so evident for the IVS-R1 sessions

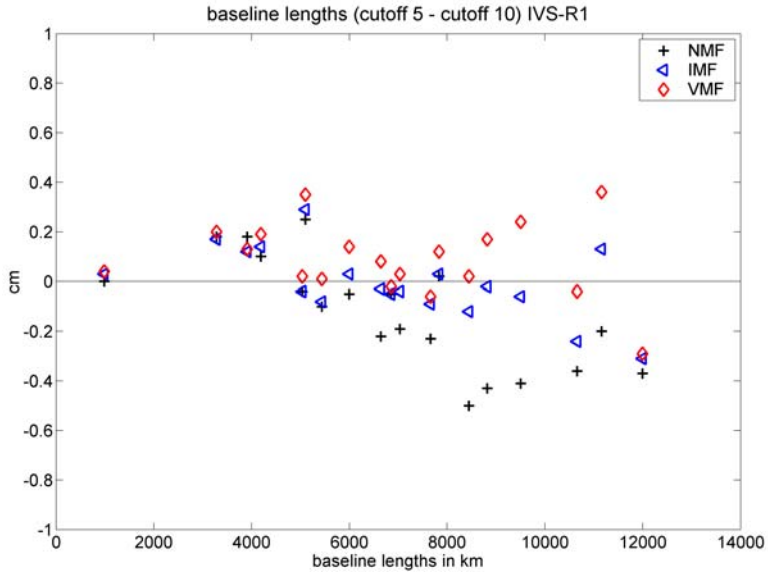

Figure 5a: Elevation angle cutoff test for IVS-R1 with NMF, IMF and VMF (fast). Baseline lengths with a 5° cutoff elevation angle are compared to baseline lengths with a 10° cutoff elevation angle.

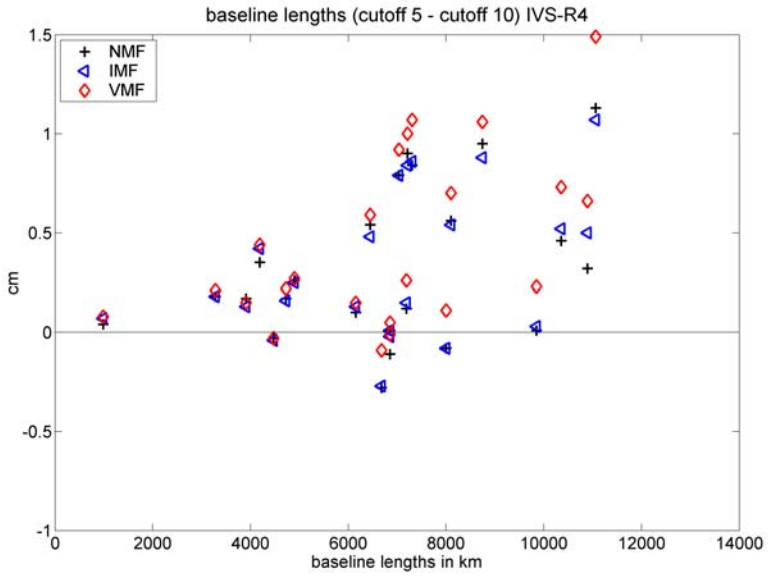

Figure 5b: Elevation angle cutoff test for IVS-R4 with NMF, IMF and VMF (fast). Baseline lengths with a 5° cutoff elevation angle are compared to baseline lengths with a 10° cutoff elevation angle.

4 Conclusions and recommendations

Recent mapping functions such as IMF and VMF based on data from numerical weather models like ECMWF provide better repeatabilities of baseline lengths and station heights than the NMF. However, systematic effects become visible which have to be investigated. Possibly, the modelling of tropospheric gradients has to be revised, too. Contrarily to IMF, the Vienna mapping functions VMF (especially the rigorous approach) exploit the information from NWMs completely and will be improved with every improvement in the NWM.

Appendix A: Raytracing

Assuming azimuthal symmetry the values for the hydrostatic and wet mapping functions as well as the outgoing elevation angle can be derived rather easily from radiosonde data or NWMs. In the following description it is referred to EMCWF pressure level data, but the considerations are valid for radiosonde data as well.

A1 Increase of the vertical resolution

ECMWF pressure level data comprise heights h in m, temperatures T in K and values for the water vapour pressure e in hPa at 15 distinct pressure level. The pressure values are [1000, 925, 850, 700, 500, 400, 300, 250, 200, 150, 100, 70, 50, 30, 10] hPa, approximately ranging from the surface of the Earth to 30 km in height. To calculate the raytracing with sufficient accuracy, the increments for the integration (distance between the pressure levels) have to be decreased and values above the 10 hPa pressure level data have to be extrapolated because the latter are significant for the light bending and the hydrostatic delay. Following Rocken (2001) height dependent increments are used (Table A1).

Table A1: Increments for the raytracing according to Rocken (2001).

Height	increment
0 km - 2 km	10 m
2 km - 6 km	20 m
6 km - 16 km	50 m
16 km - 36 km	100 m
36 km - 136 km	500 m

Linear interpolation is used for the temperature values between the 15 pressure levels. Above the 10 hPa pressure level the temperature values are taken from a standard model for the atmosphere. The values for the total pressure p and the water vapour pressure e are determined using an exponential approach.

$$p = p_0 \cdot e^{(h-h_0)/c} \qquad \text{(A1)}$$

p_0 and h_0 are the pressure and the height at the adjacent pressure level below and c is a coefficient that has been determined from the adjacent pressure levels above and below. Figure A1 shows an example for the increase of the vertical resolution. There, 15 ECMWF pressure levels have been expanded to 979 levels.

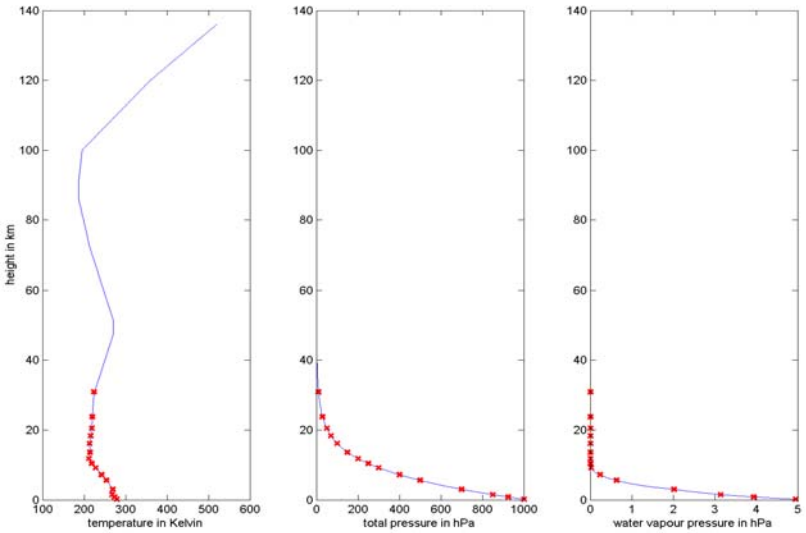

Figure A1: ECMWF pressure level data at the VLBI station Algonquin Park (Canada) on October 15, 2002 at 0:00 UT. The crosses mark the 15 pressure levels with temperature, total pressure and water vapour pressure. In between and above additional values were determined.

A2 Refractivity

At the approximately 1000 levels, the total, hydrostatic and wet refractivities have to be determined. The first is used to calculate the bending and the latter are applied to derive the hydrostatic and wet path delays, respectively. At first, the densities of the dry part (ρ_d) and of the wet part (ρ_w) are determined.

$$\rho_d = (p - e)\frac{M_d}{R}\frac{1}{T} \tag{A2}$$

$$\rho_w = e\frac{M_w}{R}\frac{1}{T} \tag{A3}$$

R is the general gas constant, and Md and Mw are the molar masses of dry air and water, respectively. The total density is the sum of the partial densities (A4).

$$\rho = \rho_d + \rho_w \tag{A4}$$

Applying the equations above the hydrostatic and wet refractivities, N_h and N_w, at each layer can be calculated.

$$N_h = k_1\frac{M_d}{R}\rho \tag{A5}$$

$$N_w = k_3\frac{e}{T^2} + k'_2\frac{e}{T} \tag{A6}$$

It has to be mentioned that the wet term in A3 does not correspond to the wet term in A6 because of the difference between the hydrostatic and the dry term. The coefficients k_1, k'_2 and k_3 are empirically determined values. The total refractivity N is the sum of the hydrostatic and wet refractivity yielding the refractive index n.

$$N = (n-1)\cdot 10^6 = N_h + N_w \tag{A7}$$

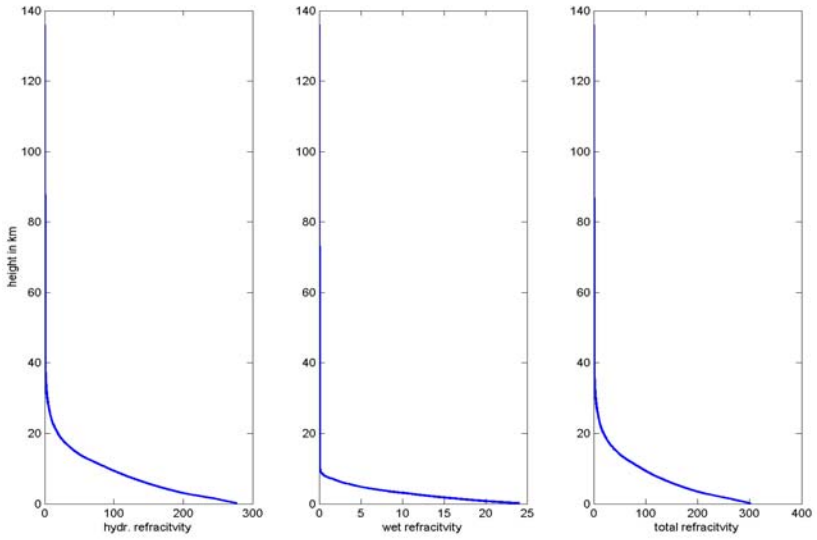

Figure A2: Values for the hydrostatic, wet and total refractivities, calculated at 979 heights above the VLBI-station Algonquin Park (Canada) on October 15, 2002, at 0:00 UT. Although the refractivities are rather small above 30 km they need to be taken into account.

Finally, the levels are cut off at the actual station height, so that there are no levels apparently below the surface of the Earth contributing to the path delays.

A3 Calculation of the raytracing

At first, it will be summarized which data are available now: At k levels (~1000) there are values for the hydrostatic and wet refractivities and for the refractive index. These are used to determine the (k–1) refractivities N_h, N_w and n in between the levels for the respective shells (see Figure A3) by simply taking the mean. Then the distances to the geocenter are determined by adding the radius of the Earth r_0 to the heights of the levels.

$$r_i = r_0 + h_i \ldots \qquad i = 1, .. k \tag{A8}$$

If the initial elevation angle e_1 is known, one gets for point P1 (see Figure A3)

$$\theta_1 = e_1 . \tag{A9}$$

Then, the distance from the first to the second point is determined with

$$s_1 = -r_1 \sin\theta_1 + \sqrt{r_2^2 - r_1^2 \cos^2\theta_1} \tag{A10}$$

and the geocentric coordinates of P1 and P2 are

$$\begin{aligned} z_1 &= r_1 & y_1 &= 0 \\ z_2 &= z_1 + s_1 \sin e_1 & y_2 &= y_1 + s_1 \cos e_1 . \end{aligned} \tag{A11}$$

The corresponding angles at the geocenter are

$$\begin{aligned} \eta_1 &= 0 \\ \eta_2 &= \arctan\left(y_2 / z_2\right). \end{aligned} \tag{A12}$$

Applying Snell's law the angles θ_2 and e_2 at the point P2 can be determined.

$$\theta_2 = \arccos\left(\frac{n_1}{n_2}\cos\left(\theta_1 + \eta_2\right)\right) \tag{A13}$$

$$e_2 = \theta_2 - \eta_2 \tag{A14}$$

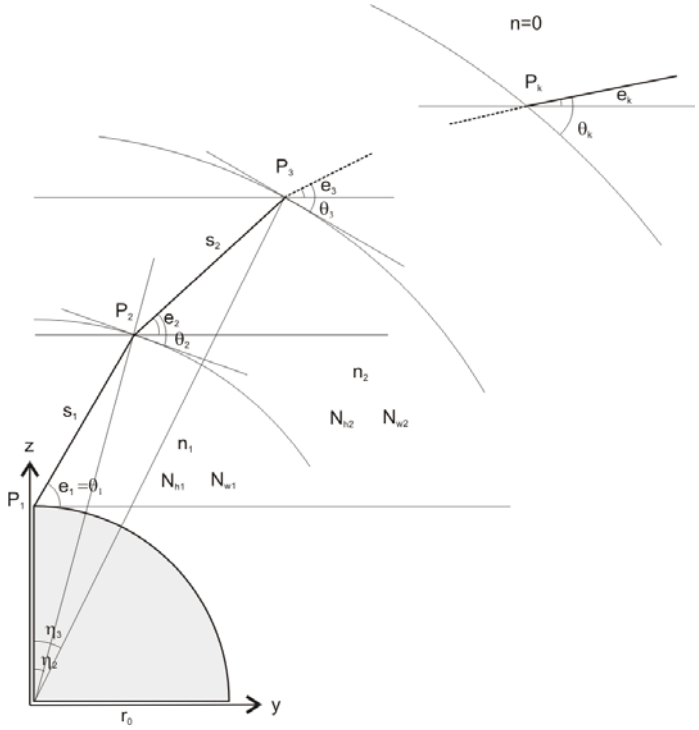

Figure A3: Raytracing.

For all other shells a loop can be set up running from 2 to (k–1).

$$s_i = -r_i \sin\theta_i + \sqrt{r_{i+1}^2 - r_i^2 \cos^2\theta_i} \tag{A15}$$

$$z_{i+1} = z_i + s_i \sin e_i \qquad y_{i+1} = y_i + s_i \cos e_i \tag{A16}$$

$$\eta_{i+1} = \arctan\left(y_{i+1}/z_{i+1}\right) \tag{A17}$$

$$\delta_{i+1} = \eta_{i+1} - \eta_i \tag{A18}$$

$$\theta_{i+1} = \arccos\left(\frac{n_i}{n_{i+1}}\cos\left(\theta_i + \delta_{i+1}\right)\right) \tag{A19}$$

$$e_{i+1} = \theta_{i+1} - \eta_{i+1} \tag{A20}$$

Applying the equations above, all incremental distances s_i between the points and the outgoing elevation angle e_k are known. Then, the hydrostatic ds_h and the wet path delays ds_w along the bended ray can be determined by summation.

$$ds_h = \sum_{i=1}^{k-1} s_i N_{hi} \tag{A21}$$

$$ds_w = \sum_{i=1}^{k-1} s_i N_{wi} \tag{A22}$$

Analogously, the path delays in zenith direction are derived.

$$dz_h = \sum_{i=1}^{k-1} dh_i N_{hi} \tag{A23}$$

$$dz_w = \sum_{i=1}^{k-1} dh_i N_{wi} \tag{A24}$$

A4 Determination of the mapping functions

The path delay used with space geodetic techniques (GPS, VLBI) does not only consist of the path delay along the bended ray but also of the geometric bending effect dgeo itself. It can be determined by

$$dgeo = \sum_{i=1}^{k-1} \left[s_i - \cos\left(e_i - e_k\right) \cdot s_i\right] \tag{A25}$$

This geometric effect is usually added to the hydrostatic mapping function. So, the values for the hydrostatic and wet mapping functions can be determined by

$$mf_h = \left(ds_h + dgeo\right)/dz_h \tag{A26}$$

$$mf_h = ds_w / dz_w \tag{A27}$$

Acknowledgements

We acknowledge the Zentralanstalt fuer Meteorologie und Geodynamik (ZAMG) for providing access to the ECMWF data. Also, we are also grateful to A.E. Niell for having very informative discussions about NWMs and mapping functions.

References

MacMillan D.S., Atmospheric gradients from very long baseline interferometry observations, Geophys. Res. Lett., Vol. 22, No. 9, pages 1041-1044, 1995.

Niell A.E., Global mapping functions for the atmosphere delay at radio wavelengths, JGR, Vol. 101, No. B2, pages 3227-3246, 1996.

Niell A.E., A.J. Coster, F.S. Solheim, V.B. Mendes, P.C. Toor, R.B. Langley and C.A. Upham , Comparison of Measurements of Atmospheric Wet Delay by Radiosonde, Water Vapor Radiometer, GPS and VLBI, Journal of Atmospheric and Oceanic Technology, 18, 830-850, 2001a.

Niell A.E., Preliminary evaluation of atmospheric mapping functions based on numerical weather models, Phys. Chem. Earth, 26, 475-480, 2001b.

Petrov L. and J.P. Boy, Study of the atmospheric pressure loading signal in VLBI observations, submitted to JGR, 2003.

Rocken C., S. Sokolovskiy, J.M. Johnson and D. Hunt, Improved Mapping of Tropospheric Delays, Journal of Atmospheric and Oceanic Technology, Vol. 18, pages 1205-1213, 2001.

Titov O., V. Tesmer and J. Boehm, Occam Version 5.0 Software User Guide, Auslig Technical Report 7, 2001.